AIP | The Journal of Chemical Physics

First principles-based multiparadigm, multiscale strategy for simulating complex materials processes with applications to amorphous SiC films

Saber Naserifar, William A. Goddard III, Theodore T. Tsotsis, and Muhammad Sahimi

Citation: The Journal of Chemical Physics **142**, 174703 (2015); doi: 10.1063/1.4919797
View online: http://dx.doi.org/10.1063/1.4919797
View Table of Contents: http://scitation.aip.org/content/aip/journal/jcp/142/17?ver=pdfcov
Published by the AIP Publishing

First principles-based multiparadigm, multiscale strategy for simulating complex materials processes with applications to amorphous SiC films

Saber Naserifar,[1,2] William A. Goddard III,[2] Theodore T. Tsotsis,[1]
and Muhammad Sahimi[1,a)]
[1]*Mork Family Department of Chemical Engineering and Materials Science, University of Southern California, Los Angeles, California 90089-1211, USA*
[2]*Materials and Process Simulation Center, California Institute of Technology, Pasadena, California 91125, USA*

(Received 19 February 2015; accepted 23 April 2015; published online 6 May 2015)

Progress has recently been made in developing reactive force fields to describe chemical reactions in systems too large for quantum mechanical (QM) methods. In particular, ReaxFF, a force field with parameters that are obtained solely from fitting QM reaction data, has been used to predict structures and properties of many materials. Important applications require, however, determination of the final structures produced by such complex processes as chemical vapor deposition, atomic layer deposition, and formation of ceramic films by pyrolysis of polymers. This requires the force field to properly describe the formation of other products of the process, in addition to yielding the final structure of the material. We describe a strategy for accomplishing this and present an example of its use for forming amorphous SiC films that have a wide variety of applications. Extensive reactive molecular dynamics (MD) simulations have been carried out to simulate the pyrolysis of hydridopolycarbosilane. The reaction products all agree with the experimental data. After removing the reaction products, the system is cooled down to room temperature at which it produces amorphous SiC film, for which the computed radial distribution function, x-ray diffraction pattern, and the equation of state describing the three main SiC polytypes agree with the data and with the QM calculations. Extensive MD simulations have also been carried out to compute other structural properties, as well the effective diffusivities of light gases in the amorphous SiC film. [http://dx.doi.org/10.1063/1.4919797]

I. INTRODUCTION

Many materials are fabricated by temperature-controlled thermal decomposition of polymers. They include porous amorphous carbon films, silicon carbide (SiC), silicon nitride, and aluminum nitride and have many important applications.[1] SiC, for example,[2] has high fracture toughness and withstands high temperatures and has many applications, ranging from electronic devices and sensors, to structural materials, automobile parts, and thin filament pyrometry. Biocompatibility, resistance to acidic and alkali environments, and chemical inertness have also made SiC a promising material for fabrication of nanoporous membranes[3] for separation of gas and liquid mixtures in harsh environments. SiC nanotubes are also being studied as storage medium for H_2 and CH_4.[4,5]

A particular class of materials that is of interest to us in the present paper is amorphous SiC films, which are fabricated[6] by pyrolysis of a partially allyl-substituted hydridopolycarbosilane (HPCS) and by chemical vapor deposition (CVD) using HPCS. Fundamental understanding of any phenomenon involving amorphous SiC (and similar materials) entails having an accurate atomistic model of the material. The most realistic route to developing such a model is one that mimics the process that produces SiC film. Since chemical reactions are also involved, the atomistic modeling requires reactive force fields (RFFs) that, in conjunction with molecular dynamics (MD) simulations, can mimic the actual processes.

To obtain a fundamental understanding of the pyrolysis process that leads to the formation of amorphous SiC film, we have carried out detailed atomistic simulations. But, because the size of the polymers used in the pyrolysis is large, modeling of the process using *ab initio* methods is computationally prohibitive. Therefore, we have developed a RFF to match our extensive quantum mechanical (QM) calculations, carried out with small systems, in order to estimate the parameters of the RFF. We then used the RFF to carry out reactive MD (RMD) simulation of the pyrolysis process. As reviewed by Farah *et al.*,[7] there are currently several RFFs that are capable of simulating reactive systems. Three of the better known of such methods and RFFs are as follows.

The RFF ReaxFF was developed by van Duin, Goddard, and coworkers,[8] who used it to study the properties of a large number of reactions in metallic, ceramic, semiconductor, and polymeric materials. Another RFF is the reactive empirical bond-order potentials developed by Brenner and coworkers.[9] They utilized their RFF to study carbon materials. Nyden and Noid[10] used a conventional nonreactive FF but dynamically varied it in order to describe chemical reactions. Chemical reactions can also be simulated by the tight binding and density functional methods. The former requires prohibitive

a)Author to whom correspondence should be addressed. Electronic mail: moe@usc.edu

computations, if the atomistic size of the material to be simulated is to be large, while the latter has been used in parts of our computations, to be described below. The focus of the present paper is on RMD simulation of chemical reactions, using ReaxFF. Several empirical and semi-empirical FFs have, of course, been developed for amorphous SiC,[11,12] but they are not capable of simulating chemical reactions.

Thus, in this paper, we describe a multiparadigm, multiscale strategy for simulating the pyrolysis of a polymer, with application to the formation of amorphous SiC films. We utilize ReaxFF in order to bridge the gap between the computational methods based on QM and empirical FFs. The QM methods are, in principle, applicable to all materials but, as already pointed out, their prohibitive computational requirement makes them unsuitable for large systems with more than a few hundred atoms. But, ReaxFF makes it possible to carry out RMD simulations of large-scale reactive chemical systems with accuracy comparable to that of the QM computations but at a fraction of the computational cost. One key feature of ReaxFF is that it describes accurately bond breaking and bond formation in materials, which is why we use it in the RMD simulation of pyrolysis of a polymer. There have been a number of studies for simulating pyrolysis and thermal degradation of polymers using ReaxFF. For example, Chenoweth *et al.*[13] used ReaxFF to investigate the thermal decomposition of Poly(dimethylsiloxane). Desai *et al.*[14] studied the pyrolysis of phenolic polymer in the presence of carbon nanotubes, while Saha and Schatz studied[15] thermal decomposition of polyacrylonitrile in the carbonization process.

The rest of this paper is organized as follows. In Sec. II, we describe the essentials of ReaxFF. Section III explains the estimation of the parameters of ReaxFF using QM computations. In Sec. IV, we describe the RMD simulation of thermal decomposition of the HPCS, while Sec. V provides the details of the formation of amorphous SiC film by MD simulation. The results are presented and discussed in Sec. VI. The paper is summarized in Sec. VII.

II. THE REACTIVE FORCE FIELD

ReaxFF uses a general relationship between bond distance and bond order, on the one hand, and between bond order and bond energy, on the other hand, leading to proper dissociation of the bonds and atoms. The total energy E of a system is given by

$$E = E_{\text{bond}} + E_{\text{over}} + E_{\text{under}} + E_{\text{val}} + E_{\text{con}} + E_{\text{tor}} + E_{\text{conj}} + E_{\text{vdWaals}} + E_{\text{ES}}. \quad (1)$$

Here, E_{bond} is the bond energy, E_{over} accounts for a degree of over-coordination number that may remain in the material (e.g., the bond order of carbon cannot exceed 4), and E_{under} is the energy due to the resonance of the π-electron between attached under-coordinated atoms. The valence angle energy is E_{val}, E_{con} and E_{conj} are, respectively, the three- and four-body conjugation energies, and E_{tors} is the torsional rotational barriers energy. Finally, E_{ES} represents the energy due to electrostatic interactions.

The expression for each partial energy is parameterized by a number of parameters. Their parameterized functional forms are long and given elsewhere[8] and, thus, are not repeated here. The overall number of parameters for the HPCS is 438, of which 39 are general, 50 are computed specifically by us for the HPCS, while the remaining 349 parameters are those computed previously by van Duin, Dasgupta *et al.*[8] for Poly(dimethylsiloxane). Since we have three types of atoms in the HPCS, namely, Si, C, and H, then, there are 26 combinations of torsional angles. The torsion energy, however, contributes weakly to ReaxFF and, thus, only 9 terms out of 26 are used in the development of ReaxFF for HPCS.

III. ESTIMATION OF THE PARAMETERS

The parameters of ReaxFF are estimated so as to reproduce the first-principles QM interactions in the HPCS, by adding the SiC crystal chemistry and the QM data for systems relevant to the HPCS to the ReaxFF training set for Si materials, as described by van Duin, Strachan *et al.*[8] The QM data for the nonperiodic systems were computed by the density-functional theory (DFT) using Jaguar (version 5.5),[16] B3LYP (Becke three-parameter Lee-Yang-Parr) functional[17] and Pople's 6-311G** basis set.[18] The Mulliken charges were also computed using the same basis set.[19] The unit cells used for each SiC polytopes and, therefore, the size of the systems varied from 8 to 16 atoms. For the energy and force convergence, the convergence criteria of 10^{-6} eV and 10^{-4} eV/Å were used, respectively. The k-points were the Gamma point centered in the unit cells, and the symmetry of space groups was used. The equation of state for the β-SiC crystal structure was obtained by the DFT calculations using Quantum Espresso.[20] The generalized gradient approximation[21] was used for the exchange-correlation energy, and ultrasoft pseudopotentials were utilized to replace the core electrons[22] with a kinetic energy cutoff of 320 eV. The Monkhorst-Pack scheme[23] was used to generate the k-space grid with a spacing of 0.1 Å^{-1}.

The geometries and energies of the species and complexes in the HPCS were computed by the DFT, as were the products of the reactions. The Si—C bond energy was optimized using the dissociation pathway for the Si—C bond in $H_3Si—CH_3$ and for Si=C in $H_2Si=CH_2$. The ReaxFF parameters were computed and optimized[24] so as to minimize the differences between the energies calculated by DFT and ReaxFF. To do so, the DFT results for the singlets were used around the equilibrium bond distances. The valence angle parameters were optimized to represent the angle-changing energies, obtained from the DFT calculations for various clusters of atoms. Six valence angles in HPCS need to be accounted for, namely, Si—C—Si, Si—C—H, C—Si—H, C—C—Si, C—Si—C, and C—Si—Si. As their representative molecules, we used the triplets $H_3Si—CH_2—SiH_3$ for the first three and $H_3C—CH_2—SiH_3$, $H_3C—SiH_2—CH_3$, and $H_3Si—SiH_2—CH_3$ for, respectively, the last three. For each angle, the representative molecule's geometry was optimized with the angles of interest fixed, so as to compute the angle-changing energies (between three atoms) relative to the optimal geometry.

The accuracy of the results is typically similar to or better than that provided by the parameterized model number 3 (the PM3 method),[25] which is a semi-empirical method for QM computation of the electronic structure of molecules. ReaxFF is about 100 times faster than PM3, which in turn is about 100 times faster than the QM calculations.

IV. SIMULATION OF PYROLISIS OF THE POLYMER

The next step is RMD simulation of thermal decomposition of the HPCS that, when followed by cooling the system back to room temperature, produces amorphous SiC film. Thus, we first generated an atomistic model of the HPCS by using a modified version of the self-avoiding walk (SAW) method of Theodorou and Suter[26,27] to generate its initial structure. Three connected atoms of the HPCS' backbone were placed in random orientations in a cubic simulation cell. The HPCS was then constructed by adding one atom at a time using the modified SAW algorithm. The allowed rotational states of the successive bonds between adjacent atoms were determined from the probability distribution functions that were governed by energy considerations (see below). Periodic boundary conditions were used. The polymer-consistent force field (PCFF) was utilized to generate the molecular model of the HPCS. According to the PCFF, the total potential energy E of the polymer is given by

$$E = E_s + E_\theta + E_\phi + E_{\text{non-bond}}, \tag{2}$$

with

$$E_s = \sum_{i=1}^{4} K_i (l - l_0)^i,\ E_\theta = \sum_{i=2}^{4} H_i (\theta - \theta_i)^i,$$
$$E_\phi = \sum_{i=1}^{3} D_i (1 - \cos i\phi), \tag{3}$$

and

$$E_{\text{non-bond}} = \sum_{i,j} \frac{q_i q_j}{r_{ij}} + \sum_{ij} \epsilon_{ij} \left[2\left(\frac{\sigma_{ij}}{r_{ij}}\right)^9 - 3\left(\frac{\sigma_{ij}}{r_{ij}}\right)^6 \right]. \tag{4}$$

Here, E_s is the bond-stretching energy, with l_0 being a bond's equilibrium length, l being its actual length at any time during the simulations, and K_i being a stretching-force constant. E_θ represents the energy associated with the changes in the bonds' angles, where θ_0 is the equilibrium angle of a bond, θ is its angle during the simulation, and H_i is the corresponding force constant. The contribution of the torsional forces is represented by E_ϕ, with D_i being a force constant and ϕ_i being the dihedral angle. The parameters σ_i and ϵ_i are, respectively, the Lennard-Jones (LJ) size and energy parameters for atom i and q_i is the partial charge of i. The nonbond interactions were cut off at an interatomic distance of 12.5 Å, while a spline switching function was used between 9.5 and 12.5 Å. The cutoffs were selected carefully, based on extensive preliminary simulations, as well as our previous extensive experience with modeling of electrostatic interactions using the multipole expansion[28] and the Ewald summation[29] techniques. One may, of course, use other methods of calculating the electrostatic interactions.[30] While including corrections due to the introduction of the cutoffs would make the simulations somewhat more accurate, for the main purpose of the present work, namely, creating an initial atomistic model of the HPCS to be used with ReaxFF for modeling its pyrolysis, the cutoffs without any corrections seemed to suffice. All the parameters of the PCFF are given elsewhere[27] and need not be repeated here.

Energy minimization and MD simulations were utilized in order to generate the equilibrated atomistic model of the polymer. The density of the polymer at the beginning of the

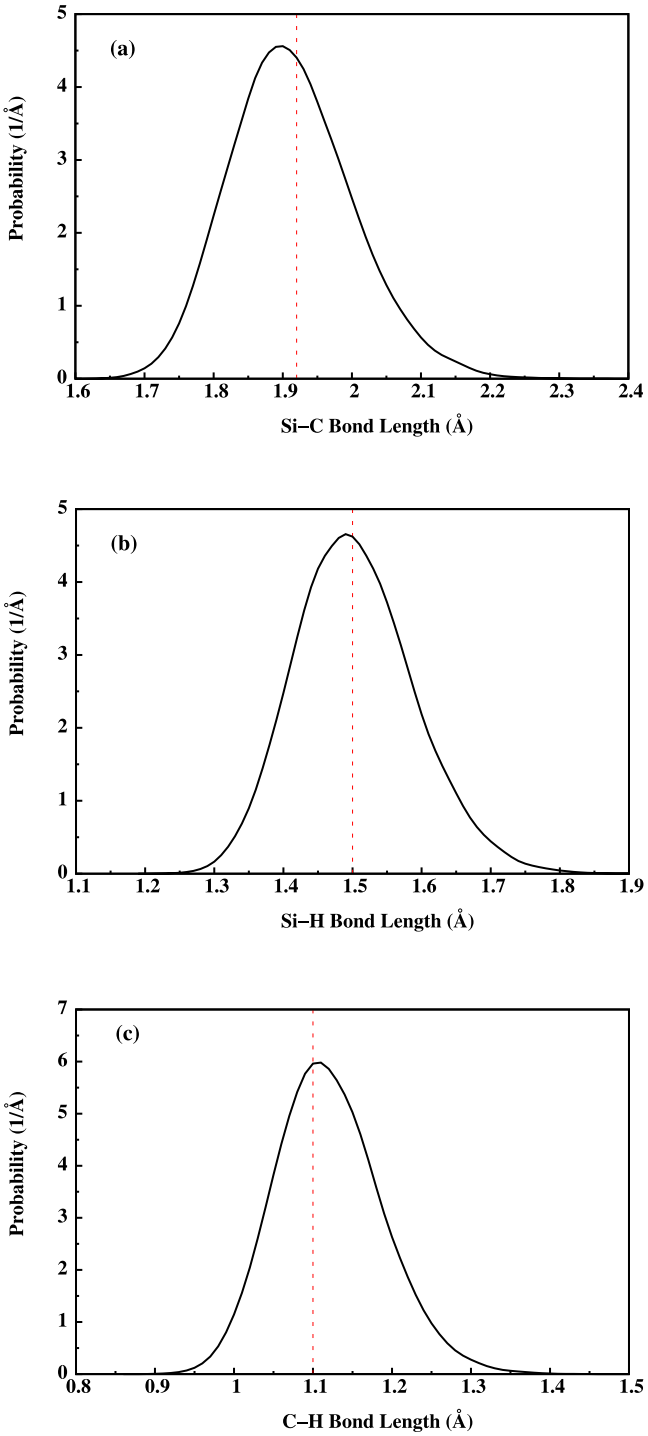

FIG. 1. The distributions of the bond length in (a) Si—C, (b) Si—H, and (c) C—H in the HPCS polymer, as generated by the PCFF. The vertical dashed lines show location of the reference bond lengths.

energy minimization was set at 0.15 g/cm^3, so as to avoid ring spearings and catenations. The total energy E of the polymer was then minimized using the conjugate-gradient method. The equilibrated structure was then compressed using MD simulation in the (*NPT*) ensemble at pressures between 0.5 and 0.6 GPa, in order to increase the polymer density to be as close to the experimental value of 0.98 g/cm^3 as possible. This was followed by energy minimization and short-duration MD simulations in the (*NVT*) ensemble at 1000 K, in order to further relax the material. Then, MD simulations were carried out in the (*NPT*) ensemble for several ns at 1 atm and 300 K. The time step was always 1 fs. The pressure was controlled by the Andersen method,[31] for which we used $W = 20$ amu for the barostat's masslike parameter. The temperature was held fixed using the Nosé-Hoover thermostat,[32] for which the parameter to scale the fictitious mass was set at 1.

To demonstrate that the PCFF generates the correct polymer structure, we show in Fig. 1 the distributions of Si—C, S—H, and C—H distances. Their maxima, corresponding to the most probable values, agree with the experimental data for the three bonds. For example, the length of the Si—C bond is 1.9 Å, in agreement with what is known experimentally. Similarly, Figs. 2 and 3 present, respectively, the distributions of the triplet angles—Si—C—Si, Si—C—H, C—Si—H, and C—Si—C—and the dihedral angles—H—C—Si—C, H—Si—C—Si, H—C—Si—H, and Si—C—Si—C—in the HPCS, and the most probable values all agree with theoretical estimates. Thus, the PCFF is capable of producing the correct molecular structure for HPCS.

The atomistic model of the HPCS was then used with ReaxFF in the RMD simulation of its thermal decomposition. The simulations were carried out in the (*NVT*) ensemble. The heating rate was 0.1 K/fs. The temperature T was gradually increased from 50 K to 5000 K. For $T < 1000$ K, the Si—H and C—H bonds are highly mobile and continuously form and break before the polymer begins to decompose. The RMD simulations indicated that the degradation of the polymer commences close to 1000 K. Since the Si—H bond is weaker than the C—H bond by about 20 kcal/mol, its cleavage initiated the decomposition process, consistent with the experimental data.[33] For $T > 1000$ K, extensive homolytic Si—H and C—H bond breaking occurred, releasing a large number of H radicals that formed bond between themselves and produced H_2 gas, the pyrolysis' primary product. SiH_n (with $n = 1$ and 2) also released H, leading to the formation of reactive silylene (=Si:) intermediates and eventually the Si—Si bonds. But, such bonds broke above 1000 K because Si tends to form more stable bonds with C.

Cleavage of the Si—C bonds began at about 2000 K and accelerated at 2400 K and higher. As a result, CH_2, SiH_2, and CH_4Si radicals formed, which then reacted with the H radicals to form CH_3, SiH_3, and CH_5Si radicals, and eventually methane, silane, and methylsilane gases. Other decomposition and reaction products included various C_2 hydrocarbons

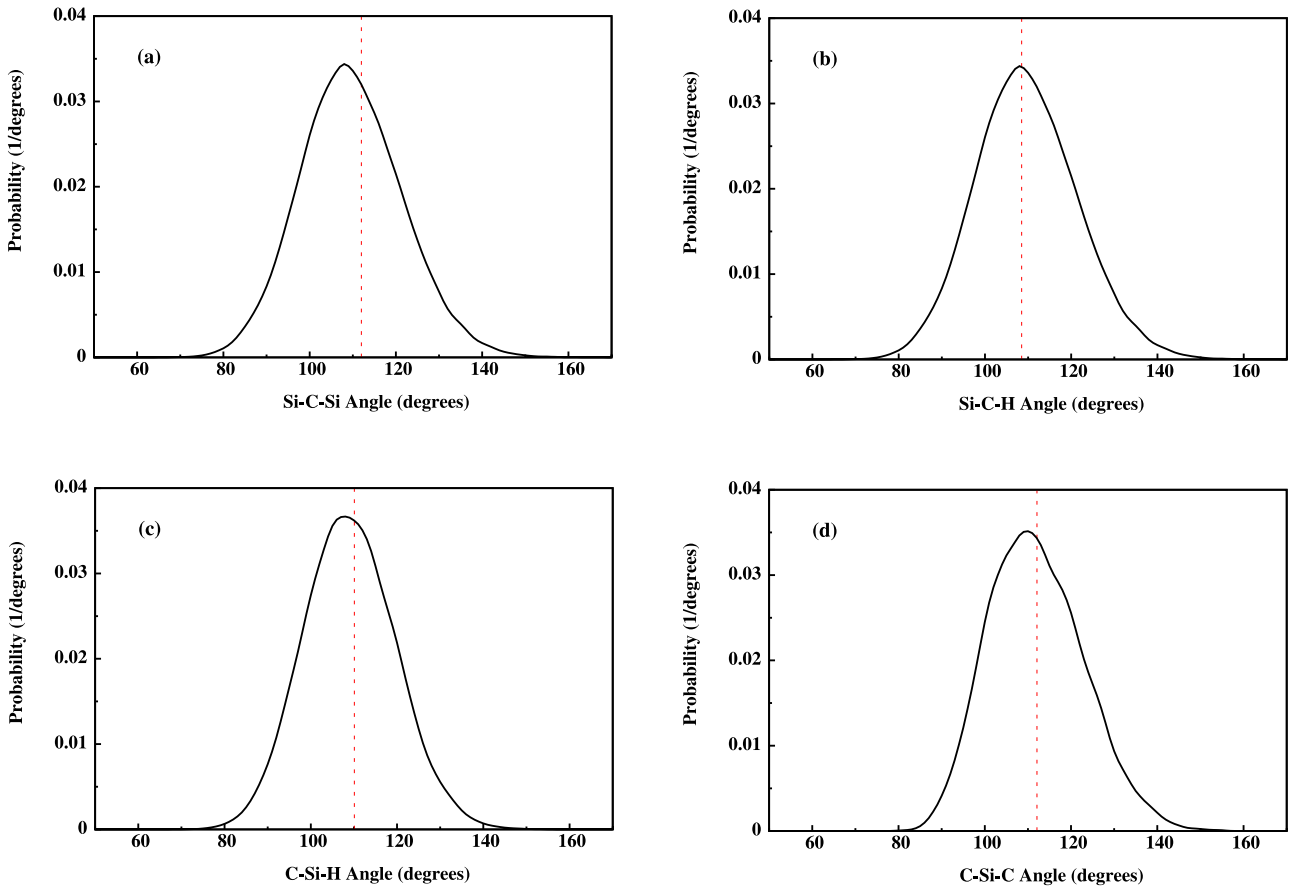

FIG. 2. The distributions of the angles in (a) Si—C—Si, (b) Si—C—H, (c) C—Si—H, and (d) C—Si—C in the HPCS polymer, as generated by the PCFF. The vertical dashed lines show location of the reference angle values.

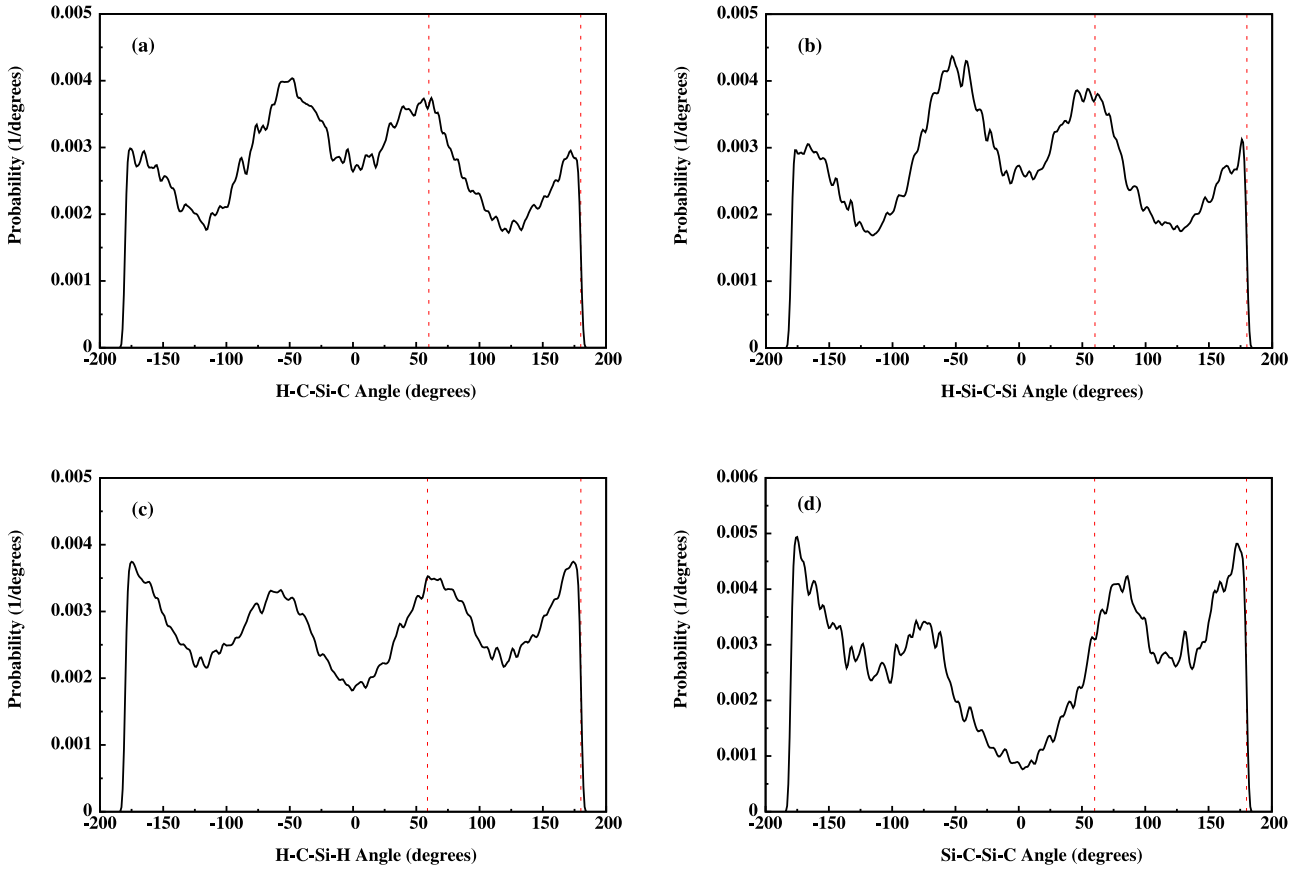

FIG. 3. The distributions of dihedral angles in (a) H—C—Si—C, (b) H—Si—C—Si, (c) H—C—Si—H, and (d) Si—C—Si—C in the HPCS polymer, as generated by the PCFF. The vertical dashed lines show location of the reference dihedral angle values.

(C_2H_6 and C_2H_4) and such radicals as C_2H_5 and C_2H_3, as well as C_2H_2.

V. FORMATION OF THE SIC AMORPHOUS FILM

Once the polymer was completely decomposed, formation of amorphous SiC was simulated by MD simulation. An important point must, however, be emphasized here. Clearly, the MD simulation can be carried for at most many nanoseconds, much shorter than the actual pyrolysis experiments that last several hours. At the same time, to capture all the changes in the geometries and charges and large variations in the density and atom connectivity, one must use short time steps; we used 0.1 fs. Therefore, the RMD simulation must be carried out at high enough temperatures in order to accelerate the computations, so that the chemical reactions can occur on the computational time scale.

A. Simulation at high temperature

Experiments[34] indicate that for $T < 1175$ K, the pyrolysis process produces amorphous SiC in which Si—H and C—H bonds break readily, releasing hydrogen radicals that eventually produce H_2, but[35] breaking of the Si—C bonds is very limited. In fact, our RMD simulation indicated that for $T < 2400$ K the Si—C bonds remain unbroken. Thus, simulation temperatures of 2400 K and lower are, roughly speaking, equivalent to the experimental temperatures of 1175 K and lower.

The reason is that experiments[33] indicated that H_2 is the major product of the pyrolysis, which is also what our RMD simulation produces. Due to being in a high energy state, free H radicals have a strong tendency to form H—H bonds. This means that if we could carry out the RMD simulations over the experimental time scales, all the H radicals would eventually react and form H_2. In the actual experiments, this takes on the order of several minutes to a few hours. Clearly, RMD simulations over such long time scales are not possible. Thus, by raising the temperature, we accelerate the formation of free H radicals and eventually H_2 molecules over the computational time scales that are currently feasible to simulate. Based on such considerations and preliminary RMD simulations, we carried out the bulk of our MD simulations in the (*NVT*) ensemble at 2000 K.

B. Incorporating insight from chemistry into the simulation

Similar to the experiments, all the gaseous products of the pyrolysis must be deleted from the simulation cell as well, but this must be done carefully. Experiments[34] indicated that H_2 is the major product of the pyrolysis, which is also what our RMD simulation produces. Thus, to speed up the computations, every two H atoms may be viewed as being equivalent to one H_2. In that case, deleting every two H radicals

during the RMD simulation would be equivalent with deleting one H_2 gas. Thus, we used shell programming to integrate the computer program with the GRASP package, in order to automatically delete the H radicals at 2-5 ps intervals. The external program evaluated the distance of every H atom in the system from all the neighboring atoms—C, H, and Si—and if it exceeded the equilibrium bond length between H and the corresponding neighboring atom by a factor of 1.2, it considered the H atom to be unbounded and deleted it from the simulation cell.

An important point must be emphasized here. One must be very careful about H removal and its effect on the dynamics of the system throughout the simulations. This is particularly important when the MD simulations are carried out within an ensemble in which the total number of atoms (N) is held fixed. Here, the H radicals are produced gradually during the simulations, and the number of H atoms that are removed at appropriate times is, relative to the total number of the atoms, negligible. Thus, after each removal step, the system has enough time to readjust the potential and kinetic energies and, therefore, gradual removal of the H atoms does not negatively affect the dynamics of the system that was tracked carefully throughout the simulations.

After removing all the hydrogen atoms at 2000 K, the system consisted of only Si and C atoms, which was then relaxed by MD simulation in the (*NVT*) ensemble using the GRASP at 2000 K for a sufficient time to allow for rearrangement of the atoms and cross-linking between Si and C atoms. Thus, the Si and C atoms began to bond together, with Si—C rings appearing in the structure. The potential energy of the system remained unchanged after 820 ps, implying that the system had reached its true equilibrium state. Experimentally,[36] the amorphous SiC produced at 1025 K is nearly stoichiometric with a density of 2.2 g/cm^3, containing a small percentage of hydrogen. Thus, the simulation cell was compressed to achieve the density of the amorphous SiC ceramic, using (*NPT*)-MD simulation at 2000 K. Thereafter, it was cooled down to ambient *T* with a cooling rate of 0.1 K/fs and equilibrated further to release the extra pressure and achieve equilibrium using (*NPT*)-MD simulations. Finally, simulated annealing in the (*NVT*) ensemble was utilized to surmount the energetic barriers, in a search for conformations with energies lower than the possibly local-minimum energy identified previously.

VI. RESULTS AND DISCUSSION

In what follows, we present and discuss the results, first for the reaction products of HPCS pyrolysis and then for the amorphous SiC films that the MD simulation generated.

A. Reaction products

All the computed parameters of ReaxFF are given elsewhere.[37] In Table I, we list all the reaction products generated by the RMD simulations. These are in agreement with the experimental data,[33] both qualitatively and quantitatively, for the products of the HPCS decomposition. Reference 33 reported, for example, that most of the produced gas was hydrogen, followed in much smaller quantities by CH_4, SiH_4, and other low-molecular weight gases. These are also what we obtained, as well as other gases that may not be possible to measure experimentally with any precision due to their trace amount. This is, of course, an advantage of ReaxFF. Previously, we also compared[37] the results of the QM calculations with those obtained with ReaxFF, and the two agree closely.

TABLE I. The pyrolysis products after heating up the polymer to 3600 K. *N* is the number of the produced product, and MW its molecular weight.

N	Product	MW	*N*	Product	MW
122	H	1.00	1	$C_2H_5Si_3$	113.32
26	H_2	2.00	1	$C_2H_7Si_3$	115.33
3	CH_3	15.03	3	$C_2H_{10}Si_3$	118.36
11	CH_4	16.04	1	$C_2H_{11}Si_3$	119.36
2	C_2H_4	28.05	1	$C_5H_9Si_2$	125.29
3	HSi	29.09	3	$C_3H_8Si_3$	128.35
7	H_2Si	30.10	1	$C_3H_9Si_3$	129.36
5	H_3Si	31.11	2	$C_3H_{10}Si_3$	130.37
10	H_4Si	32.12	1	$C_4H_{12}Si_3$	144.39
1	CSi	40.09	1	$C_4H_{13}Si_3$	145.40
4	CH_2Si	42.11	1	$C_2H_{12}Si_4$	148.46
14	CH_3Si	43.12	1	$C_3H_{10}Si_4$	158.45
16	CH_4Si	44.13	1	$C_3H_{11}Si_4$	159.46
10	CH_5Si	45.13	1	$C_4H_{12}Si_4$	172.48
5	CH_6Si	46.14	1	$C_4H_{13}Si_4$	173.49
1	CH_7Si	47.15	1	$C_5H_{14}Si_4$	186.50
1	C_2H_2Si	54.12	1	$C_3H_{15}Si_5$	191.58
1	C_2H_3Si	55.13	1	$C_4H_{13}Si_5$	201.57
3	C_2H_5Si	57.14	1	$C_4H_{14}Si_5$	202.58
3	C_2H_6Si	58.15	1	$C_4H_{15}Si_5$	203.59
1	C_2H_7Si	59.16	1	$C_5H_{15}Si_5$	215.60
1	CH_4Si_2	72.21	1	$C_5H_{19}Si_5$	219.63
2	CH_5Si_2	73.22	1	$C_6H_{16}Si_5$	228.62
4	CH_6Si_2	74.23	2	$C_7H_{16}Si_5$	240.63
1	CH_7Si_2	75.24	1	$C_5H_{15}Si_6$	243.69
3	$C_2H_5Si_2$	85.23	1	$C_6H_{19}Si_6$	259.73
3	$C_2H_6Si_2$	86.24	1	$C_6H_{19}Si_7$	287.81
4	$C_2H_7Si_2$	87.25	1	$C_8H_{25}Si_7$	317.88
1	$C_2H_8Si_2$	88.25	1	$C_9H_{20}Si_8$	352.94
2	$C_2H_9Si_2$	89.26	1	$C_{14}H_{37}Si_{12}$	542.47
1	$C_2H_{10}Si_2$	90.27	1	$C_{14}H_{39}Si_{13}$	572.57
1	$C_3H_8Si_2$	100.27	1	$C_{17}H_{42}Si_{13}$	611.63
2	$C_3H_9Si_2$	101.27			

Figure 4 presents the "pie chart" for all the radicals and molecules produced at 3600 K. Consistent with experiments, hydrogen radicals constitute the major component of the reaction products, hence explaining why H_2 is the most important product of the pyrolysis. This is followed by $C_nH_pSi_m$ that eventually produce CH_4 and SiH_4 and trace amounts of other gaseous compounds. The same type of chart is obtained at other high temperatures. Such charts also explain the formation of Si—C covalent bonds by cross-linking of long chains $C_nH_pSi_m$ and loss of hydrogen.

Figure 5 presents the evolution of the production of SiH_n radicals with $n = 1 - 4$ during the pyrolysis of the HPCS at 3200 K. There are large fluctuations since the radicals lose their hydrogen, but because the system is highly reactive, they also form bonds with the hydrogen radicals, giving rise

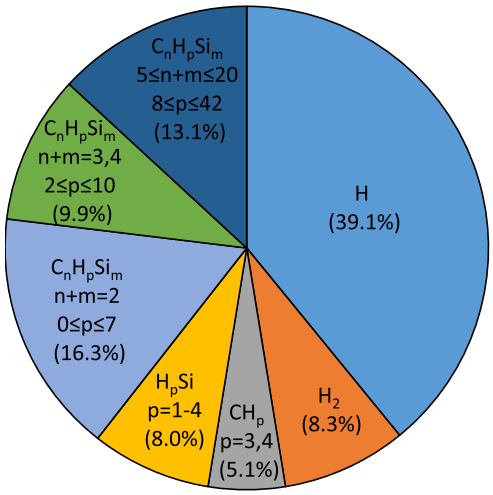

FIG. 4. The "pie chart" for the radicals and molecules produced during pyrolysis of HPCS polymer at 3600 K.

to the fluctuations. Some clear trends can also be discerned. The number of SiH is always very small, followed by SiH_2. Some of the two radicals are of course converted to SiH_3 and SiH_4 and some lose all of their hydrogen, leaving Si to form covalent bond with carbon. Similar trends were observed for CH_n ($n = 1 - 4$) and, thus, are not shown.

Figure 6 presents the same as in Fig. 5, but at 4000 K. Once again, the number of the SiH is small, but larger than what is produced at 3200 K. The fluctuations in the number of SiH_n with $n = 2 - 4$ are also larger than those at 3200 K. Figure 7 presents the results for CH_nSi, with $n = 1 - 6$, at 4000 K. As expected, the number of CHSi is low, while after an initial "burst," the number of produced CH_nSi with $n = 2 - 4$ clearly decays with time, since they are decomposed at such a high temperature.

We also studied the kinetics of H_2 formation. In Fig. 8, we show the raw data for the time-dependence of the number of H_2 produced, $N(t)$, at 3000 K, as well as their smoothed version. Also shown is the fit of the smoothed data to the functional form,

$$N(t) = N_f - (N_f - N_0)\exp(-kt), \quad (5)$$

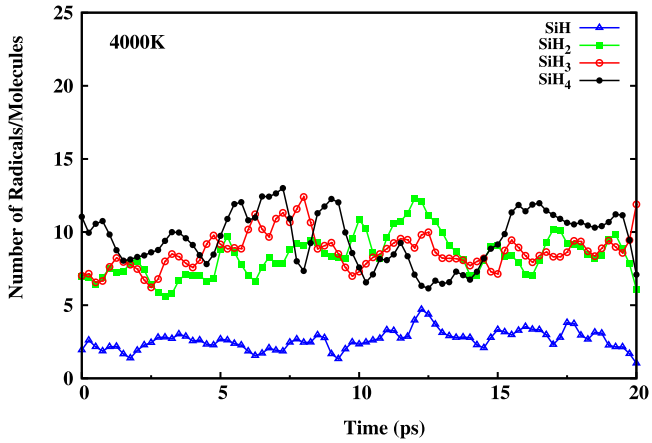

FIG. 6. Same as in Fig. 4, but at 4000 K.

where N_0 and N_f are the initial and final number of produced H_2 in the simulation and k is a kinetic constant in ps^{-1}. Except for early times, the functional form provides a reasonable fit of the smoothed data. Note that the methodology of removing H radicals does not have any significant effect on the dynamics and the quality of the final products, which was confirmed by comparing with experimental data. Thus, Fig. 7 presents the general trends of H_2 production.

B. Properties of the SiC film

The density of SiC ceramic resulting from the pyrolysis of the HPCS has been reported[38] to be 2.2 g/cm^3. The final structure from the RMD and then MD simulations also has the same density.

The three major SiC polytypes are[1,2] (β) 3C-SiC, (α) 6H-SiC, and 4H-SiC. The Crystal Builder module in Cerius2[39] and its associated unit cell parameters[40] were used to construct the SiC crystals. For each crystalline form, the quantum energies were computed in order to describe both expansion and compression. Figure 9 compares the ReaxFF results with those obtained by the DFT. Optimization of β-SiC crystal with ReaxFF yielded a density of 3.16 g/cm^3 at 300 K, compared with the experimental value, 3.21 g/cm^3.

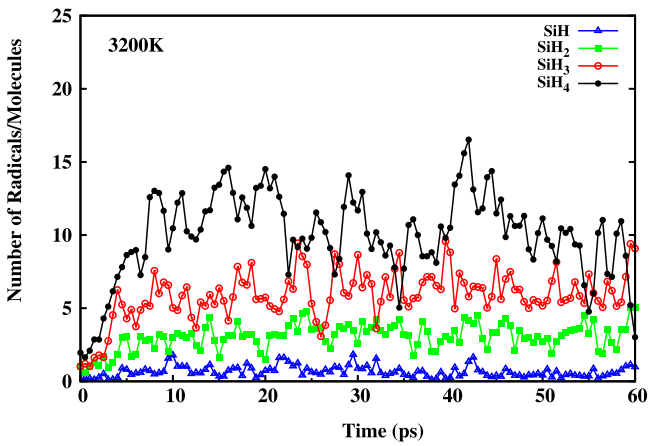

FIG. 5. Time-dependence of production of SiH_n during MD simulation in the (NVT) ensemble at 3200 K.

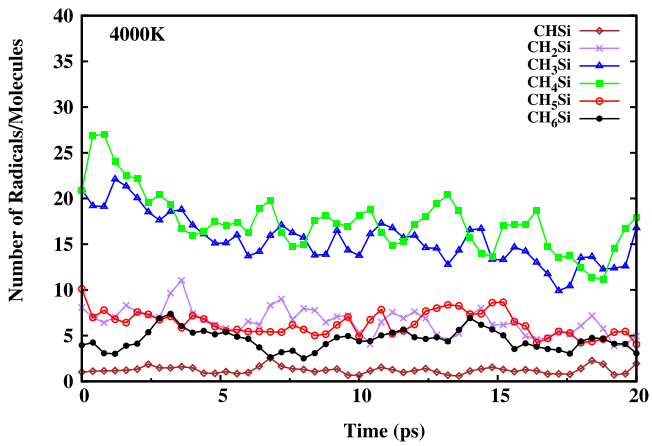

FIG. 7. Time-dependence of production of CH_nSi during MD simulation in the (NVT) ensemble at 4000 K.

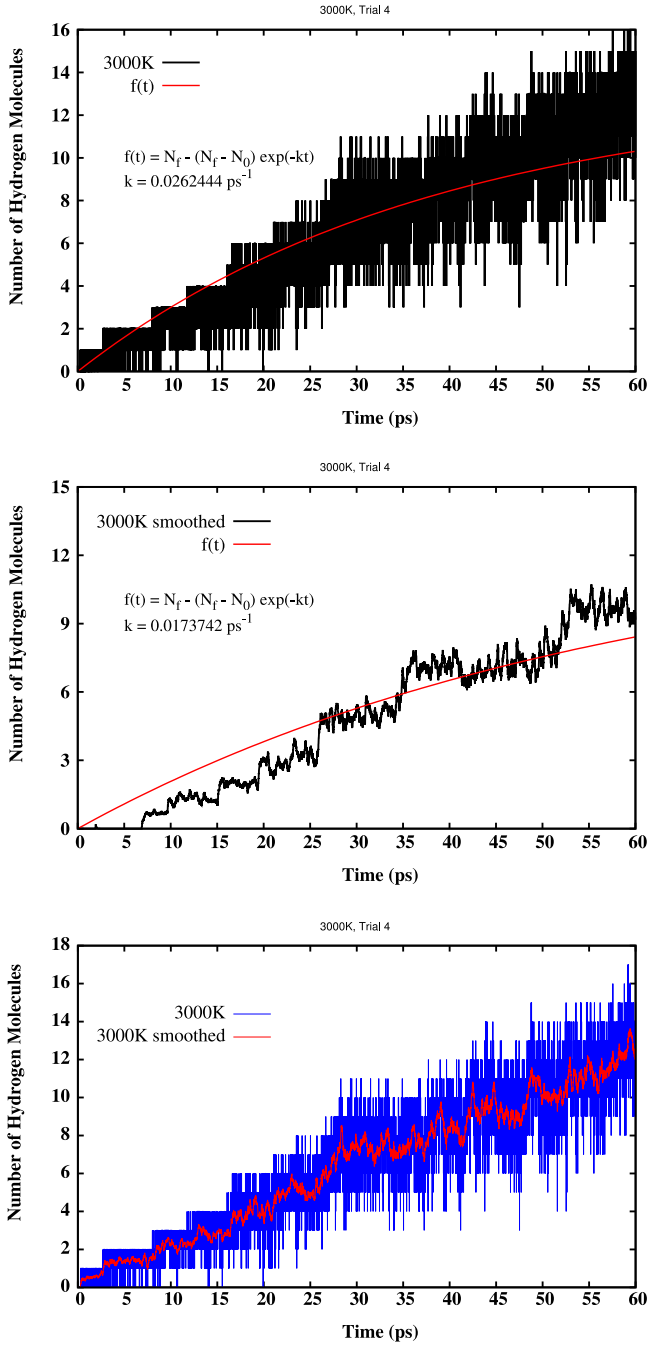

FIG. 8. Temperature-dependence of the rate of production of H_2 according to both the original and smoothed data (top), the fitted curve against the original (middle), and against the smoothed data (bottom). The results are for 3000 K.

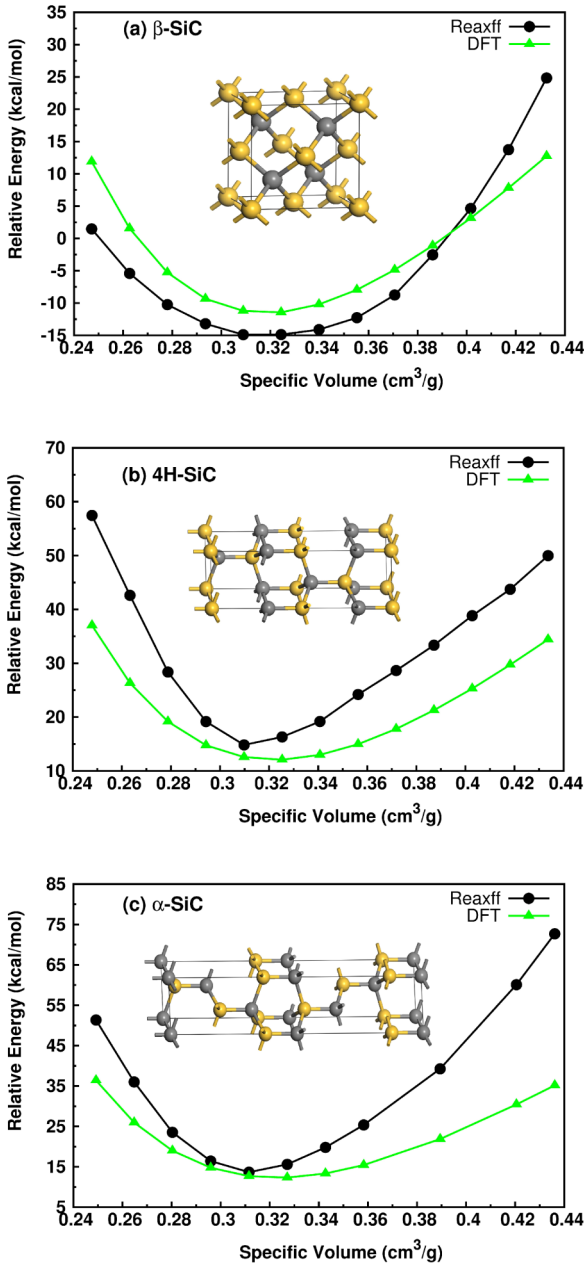

FIG. 9. The equations of state (compression and expansion) for the three crystal structures of SiC. (a) β-SiC, (b) 4H-SiC, and (c) α-SiC, as computed by the DFT and ReaxFF.

Figure 9 indicates, for large expansions, significant difference between the energies computed by ReaxFF and the DFT. This does not, however, cause a problem for the phenomenon of interest to us in this paper because the most relevant and physically interesting parts are the equilibrium volumes from which the relative phase stabilities are deduced. We also point out that the important point in using ReaxFF is to enable chemical reactions to proceed with appropriate energy barriers. Thus, ReaxFF uses a bond energy-to-bond order-to bond distance relation that captures double and single bonds, as well as lower-order bonds during the reactions. As a result, the compressibility curves computed by ReaxFF are generally not as accurate as one would like them to be. For covalent systems, calculations of accurate second-order properties are best carried out by using ReaxFF to obtain the structure, and then one should use a *nonreactive* FF to analyze the distortions near the equilibrium structure.

We also computed[41] the radial distribution function $g(r)$ of the final SiC film at 300 K and compared it with the data[42] at 300 K. Generally speaking, the agreement between the computed $g(r)$ and the data is good. In particular, both the data and the atomistic model of amorphous SiC indicate the existence of some Si—Si and C—C in the material. As we reported previously,[41] there are only some small differences between the computed and experimental $g(r)$. The reason is, in order to observe the reactions in computational time scale, we accelerated the reactive dynamic simulation,

as described earlier. This meant using higher heating rate and higher pyrolysis temperatures, when compared with the experiment. The difference has some minor effect on the quality of the output SiC and, therefore, some minor differences in the radial distribution function. The structure of the amorphous SiC film was further validated by computing its x-ray diffraction pattern. Comparison[41] with the data[43] also indicated good agreement between the computed and measured x-ray diffraction patterns.

Study of flow and transport of fluids in confined media, and in particular in nanoporous media, is currently of fundamental and practical interest. The reason is threefold. First, the energy dissipation caused by friction in confined fluid can change the chemistry of the process and, in addition to forming new components, phase transitions as well as drastic changes in the fluid's static and dynamical properties also occur, which are phenomena of fundamental importance that can be very different from those under the bulk conditions. Second, it is clearly of practical interest to understand the mechanism of transport in the pore space of nanoporous materials. Third, the morphology of such materials is characterized and better understood by studying transport (and adsorption) in their pore space.

One particular class of nanoporous materials of interest to us contains pores with an average size of about a few Å. Due to such exceedingly small pore sizes that are comparable with those of the fluids typically passing through them, the main resistance to the flow and transport in nanoporous material is due to the nano- and mesopores and, therefore, the molecular interactions between the gases' molecules, as well as between them and the pores' walls, are important and cannot be ignored. Hence, one must utilize atomistic modeling and simulation to study the transport processes that take place in the pore space of such materials. We have been fabricating various types of nanoporous materials for use as membranes, such as carbon molecular-sieve membranes,[44] nanotube-polymer composites,[27] and SiC nanoporous membranes.[3]

Thus, having established the accuracy of ReaxFF for simulating the pyrolysis of HPCS and the atomistic model of amorphous SiC film, we now turn our attention to the properties of the amorphous SiC film that is produced by the pyrolysis process, after the system is cooled back to room temperature. Amorphous SiC films have been used by us[3] as the membrane layer for separation of gaseous mixtures into their constituents. Thus, we are interested in the free-volume distribution of the films and the effective diffusivities of various gases in the SiC films.

(1) *The force field*: We computed the self-diffusivities of three gases in the SiC film, namely, H_2, CO_2, and CH_4, because the SiC nanoporous films are used for separation of mixtures of the three gases.[3] To do so, one must specify the interaction potentials between the gases and the SiC film. For this purpose, we used the universal force field[45] (UFF). The parameters of the UFF have been estimated according to general rules based only on the atomic element, its connectivity, and hybridization. The total energy E according to the UFF is given by

$$E = E_s + E_\theta + E_\phi + E_\omega + E_{\text{vdWaals}} + E_{\text{ES}}, \tag{6}$$

with

$$\begin{aligned} E_s &= \frac{1}{2} S_{ij} (\ell - \ell_{ij})^2, \\ E_\theta &= T_{ijk} \sum_{n=1}^{m} C_n \cos(n\theta), \\ E_\phi &= P_{ijkl} \sum_{n=1}^{m} C_n \cos(n\phi_{ijkl}), \\ E_\omega &= G_{ijkl} [C_0 + C_1 \cos\omega_{ijkl} + C_2 \cos(2\omega_{ijkl})], \\ E_{\text{vdWaals}} &= V_{ij} \left[\left(\frac{r_{ij}}{r} \right)^{12} - 2 \left(\frac{r_{ij}}{r} \right)^{6} \right], \\ E_{\text{ES}} &= 332.0637 \frac{q_i q_j}{\epsilon r_{ij}}. \end{aligned} \tag{7}$$

Here, E_s is the energy associated with bond stretching, with ℓ_{ij} being the equilibrium or natural bond length, ℓ being the actual length at any time during the simulation, and S_{ij} being a stretching-force constant. E_θ represents the energy associated with the changes in the bonds' angles, where the coefficients C_n are chosen to satisfy the appropriate, physically justified boundary conditions where the function has a minimum at an equilibrium bond angle θ_0, θ is the angle at any given time during the simulation, and T_{ijk} is the corresponding force constant. The contribution of the torsional forces is represented by E_ϕ, with P_{ijkl} being a force constant. Values of P_{ijkl} and the coefficients C_n are determined by the rotational barrier V_ϕ, the periodicity of the potential, and the equilibrium angle. For a given central $j - k$ bond, all torsions about this bond are considered, with each torsional barrier being divided by the number of torsions present about the bond. E_ω represents the energy associated with the inversion, with G_{ijkl} being a force constant and ω_{ijkl} being the angle between the il axis and the ijk plane. E_{vdWaals} is the van der Waals type potential represented by a LJ 6-12 type potential for the nonbond interactions, with V_{ij} being the well depth and r_{ij} being the van der Waals bond length. The general r_{ij} and V_{ij} are obtained from the homonuclear parameters through the use of combination rules

$$\begin{aligned} r_{ij} &= (r_i r_j)^{1/2}, \\ V_{ij} &= (V_i V_i)^{1/2}. \end{aligned} \tag{8}$$

Finally, E_{ES} represents the energy associated with the electrostatic interactions, where q_i is the atomic charge. In the simulations, the potential energy for the nonbonded interactions was cut off at 6 Å. We used the Ewald summation technique and the multiple expansion method[28,46] in order to account for the electrostatic interactions. All the parameters of the UFF are given in the original reference.[45]

(2) *Computing the accessible free volume and solubility*: The free-volume (FV) distribution is important to transport of the gases through the SiC films. To compute the FV distribution, MD simulations in the (*NPT*) ensemble were carried out. Twenty configurations of the SiC film structures were taken from the simulation trajectories after every 50 fs. The accessible FVs were then computed using the following method using a hard-sphere probe. First, the cubic simulation cell was partitioned into a three-dimensional mesh of

$100 \times 100 \times 100$ elementary cells. Then, a hard sphere of a given diameter was inserted as the probe at the center of each elementary cell, and the distance to the nearest atoms of the material was computed. If the distance turned out to be larger than the sum of the van der Waals radii of the penetrant molecule and the material's atom, the elementary cell was considered as contributing to the accessible free volume. The cavity volume was then computed using a Voronoi tessellation of the space based on the algorithm of Tanemura *et al.*[47] The vectors connecting the atoms' centers in the system were perpendicularly bisected and a large number of intersecting planes were generated. The polyhedra associated with the atoms were then constructed using the algorithm. As a Voronoi polyhedron around an atom identifies its own available space, it can be related to the void volume of the SiC film, which was then used to study the evolution of the free volume.[48]

(3) *Computing the self-diffusivity of the gases*: To compute the self-diffusivity of H_2, CH_4, and CO_2 in the SiC model, 10 molecules of each gas were inserted in the SiC film separately. For convenience, we use MH_2, MCH_4, and MCO_2 to denote the SiC material that contains H_2, CH_4, and CO_2, respectively. In each case, the system was constructed by adding one gas molecule at a time, in a stepwise fashion, into the SiC model. The molecules were randomly inserted in the free space of the SiC film and any physically unacceptable contact and overlap between the gaseous molecules and the atoms of the SiC model was avoided. After the insertion of every gas molecule, the total energy of the system was minimized using the conjugate-gradient algorithm. The process was followed until the desired number of gas molecules in the SiC flim was reached. To suppress the surface effects and the small size of the system, the periodic boundary conditions were used.

After generating the SiC film-containing systems, the energy of the materials was first minimized until it achieved its true minimum. To further equilibrate the structures after energy minimization, MD simulations were carried out in the (*NVT*) ensemble for 20 ps at 300 K. Then, another series of MD simulations was carried out in the (*NPT*) ensemble for several ns at 1 atm and 300 K. The time step was 1 fs. The pressure was controlled by the Andersen method,[31] while the temperature was held fixed using the Nosé-Hoover thermostat[32] (see the earlier discussions).

The cell length and density of the SiC films were about 21.4 Å and 2.2 g/cm^3, respectively. The cell lengths and densities, after energy minimization and relaxation, were about 23.7 Å and 2.22 g/cm^3 for MH_2, 24.2 Å and 2.25 g/cm^3 for MCH_4, and 23.6 Å and 2.29 g/cm^3 for MCO_2. Given the void space in the pure (without any gas) SiC film (see below), their densities appear reasonable, considering the size of the cells and the mass of the gases.

The self-diffusivity of H_2, CO_2, and CH_4 in the SiC film were estimated based on the mean-square displacements of the gas molecules using the Einstein relation,

$$D = \frac{1}{6} \lim_{t\to\infty} \frac{d}{dt} \sum_{n=1}^{N} \langle |R(t) - R(0)|^2 \rangle, \tag{9}$$

where D donates the self-diffusion coefficient and $R(t)$ is the Cartesian position vector of a gas molecule at time t.

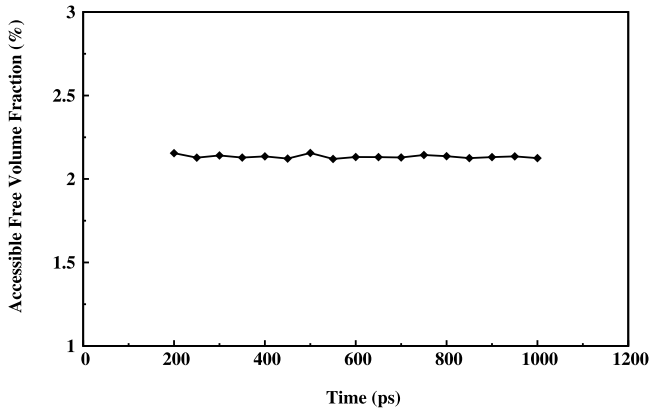

FIG. 10. Time-dependence of the accessible free volume fraction with a probe diameter of 2.5 Å.

The $\langle \cdots \rangle$ indicates averages over all the gas molecules and over all possible time origins for the motion of the molecules. The limiting slope of the mean-square displacement as a function of time is then used to evaluate the self-diffusion coefficient of a molecule undergoing random Brownian motion in three dimensions.

(4) *Accessible free volume*: The time dependence of the FV fractions f_v for a probe of size σ = 2.5 Å, averaged over 20 configurations taken from the MD simulation in the (*NPT*) ensemble, is shown in Fig. 10, indicating that the fluctuations of f_v were very small. In general, the characteristic times in the SiC model are so long that the accessible free volumes undergo very small fluctuations. Fluctuations of the accessible FVs in the MCH_4, MCO_2, and MH_2 are somewhat larger than those in the pure SiC model, which is due to the presence of the gases and the fluctuations that they induce in the FV of the pores of the SiC film. Such features indicate that the atomistic models that we have generated for the SiC model and its gaseous mixtures should be quite reasonable.

Figure 11 presents the FV fraction f_v as a function of the probe diameter, represented by its LJ size parameter σ, for the pure SiC film and MCH_4, MCO_2, and MH_2 systems. In all the cases, the f_v decrease rapidly as the probe diameter increases, and are less than 1% when the probe diameter reaches 5 Å. This indicates that the insertion of the gases in the SiC film

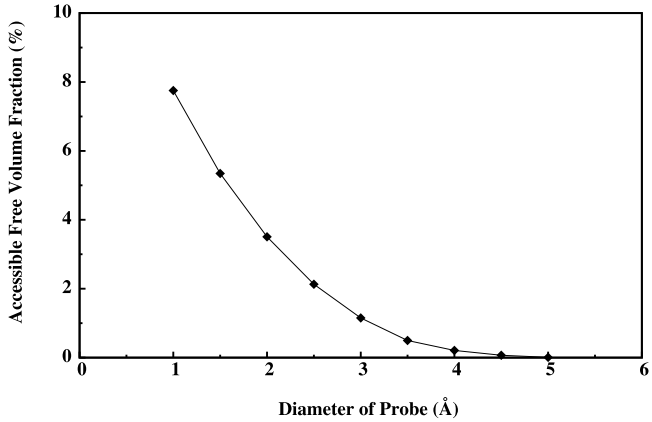

FIG. 11. The fraction of the free volume of amorphous SiC as a function of the probe size.

does not change much the percentage and shape of the larger pores that the gases can diffuse into. There is, however, a difference in the values of f_v for small probes, which is due to the repulsive interactions between the gaseous molecules and the SiC atoms and the fluctuations that such interactions induce in the material.

As described earlier, the Voronoi tessellation method was utilized to compute the distribution of the cavity sizes (volumes) for the unit cells of the SiC model, taking all the atoms into account. Figure 12 presents the resulting cavity volume distributions at three different times. They indicate that the distributions do not vary much with time, hence demonstrating the stability of the entire system. It is worth noting that there is a small but significant fraction of large cavity volumes. Considering the size and the volume of the gaseous molecules, the entire range of the cavity volumes

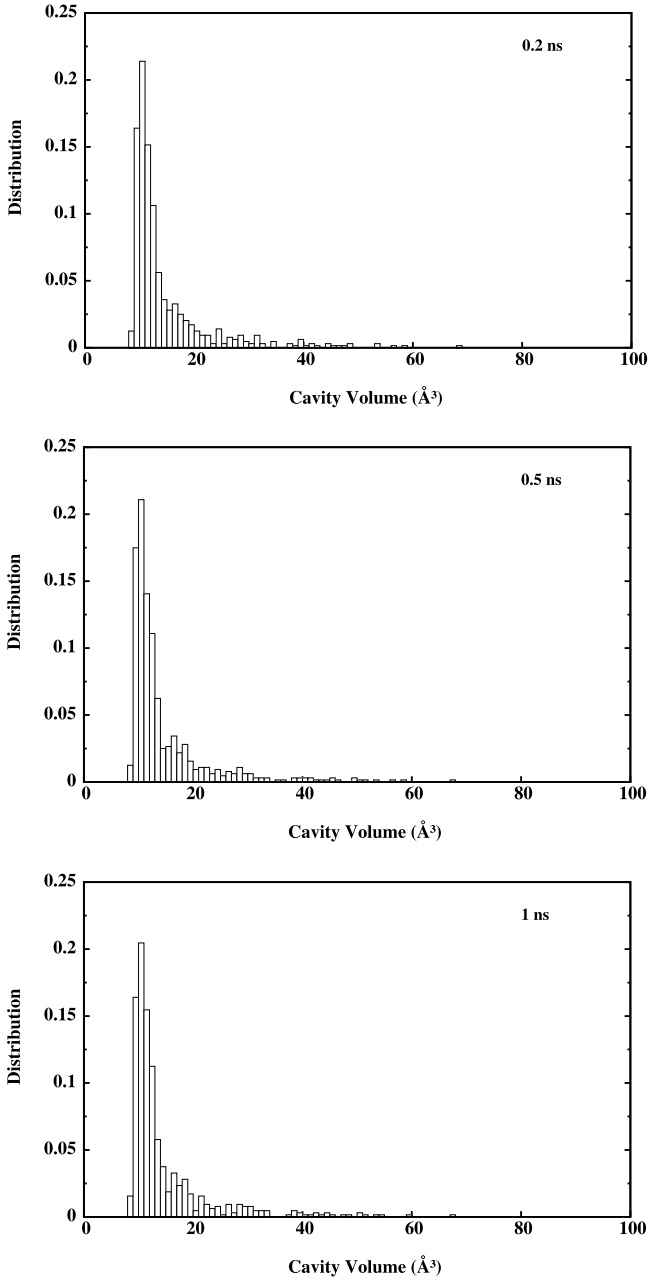

FIG. 12. The distribution of the free volumes at three different times.

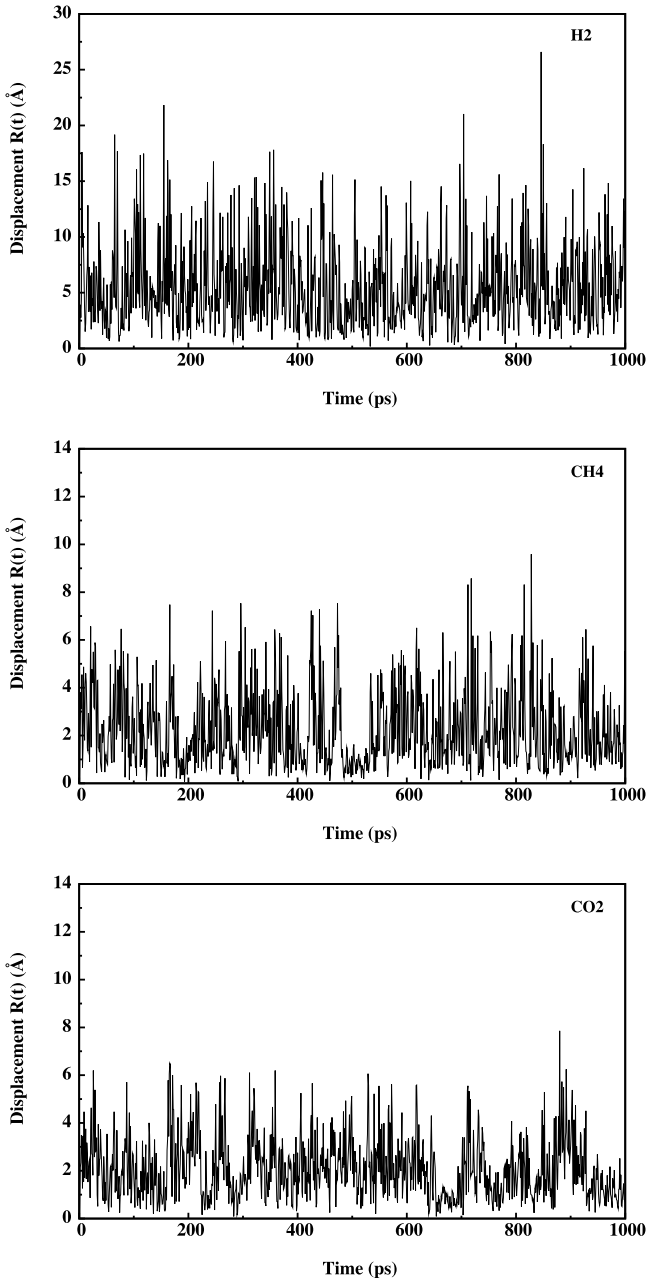

FIG. 13. Time-dependence of the displacements of the three gases relative to their last positions.

is responsible for gas permeation, diffusion, and separation, when used as a membrane or in other applications.

(5) *The self-diffusivities*: In amorphous SiC, the accessible FV for the diffusion of small gases is distributed *inhomogeneously* throughout the system. Thus, the diffusion coefficients may vary significantly *locally*. That is, they may be different if computed for various parts of the amorphous SiC film. The dependence of the diffusivities on the local FV fraction may then be described by Doolittles' law,[49]

$$D = A \exp\left(-\frac{B}{\eta_{max} - \eta}\right), \tag{10}$$

or a modification of it,[50] where η is the packing fraction of the material, with $\eta_{\max}$ being its maximum value, and A and

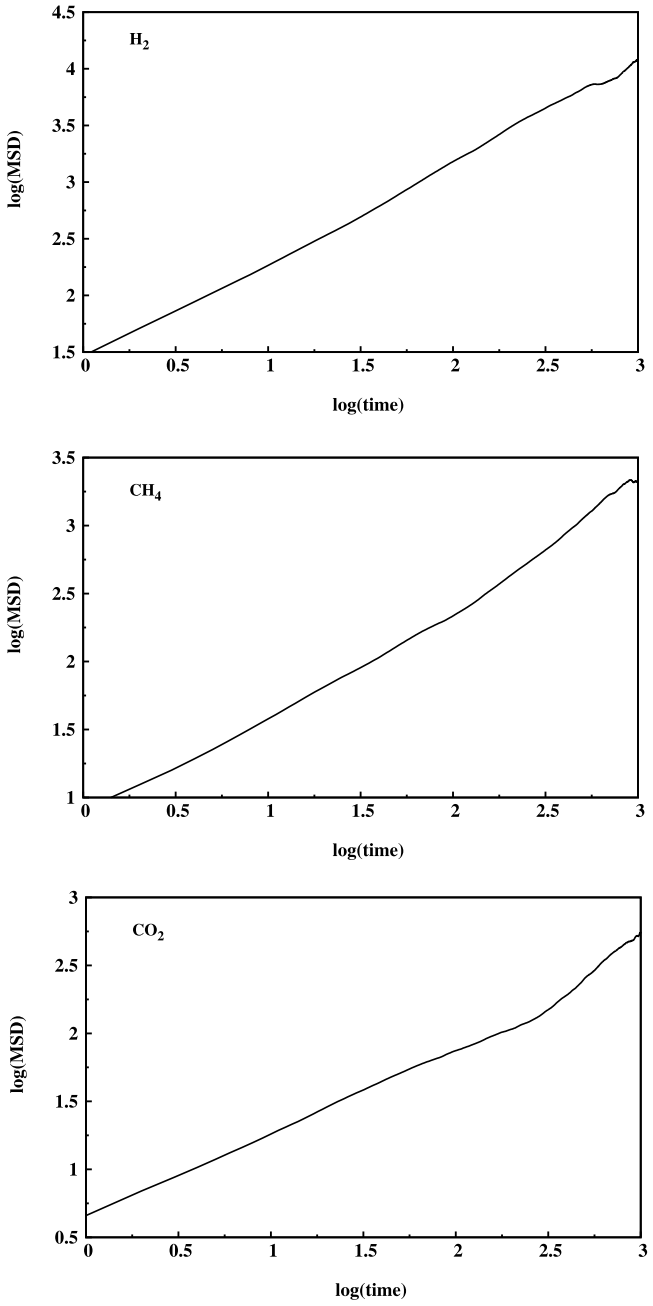

FIG. 14. Logarithmic plots of the mean-square displacements versus time of the three gases, computed in the (*NPT*) ensemble at 300 K.

B being two constants. One may also consider the Cohen-Turnbull statistical mechanical theory according to which

$$D = M \exp\left(-N\frac{v_m}{v_a}\right), \tag{11}$$

where M and N are two constants, v_m is the minimum free volume required for a diffusing molecule to escape its cage of neighboring atoms, and v_a is the available free volume per volume of the occupying element.[51] To decrease the degree of inhomogeneity for calculation of the self-diffusivities, 10 molecules of each gas were inserted in the SiC film at random positions, as described earlier.

The simulations indicated that H_2, CH_4, and CO_2 take diffusion trajectories in the SiC material that are sample-spanning paths, indicating that the SiC film's pores are large enough for the gases to diffuse through. There is, however, an important difference between the three gases: H_2 diffuses more efficiently than the other two gases. This implies that the amorphous SiC film is more favorable for diffusion and transport of H_2 and, therefore, it is an effective material for its separation from the gaseous mixtures, in agreement with the experimental data and observations.[3] The slowest molecule in the SiC film is CO_2, which may be explained not only based on being a (relatively) heavy molecule but also due to the presence of the C atoms on the pores' surface. CO_2 has some affinity for physical adsorption on the surface of pores that contain carbon, which slows down its motion.

TABLE II. The computed self-diffusivities D of the three gases.

Gas	$D \times 10^4$ (cm^2/s)
H_2	1.81
CH_4	0.39
CO_2	0.09

To better understand the difference between the three gases, we show the time-dependence of their displacements $R(t)$ in Fig. 13. The displacement of H_2 fluctuates between 1 Å (essentially vibrations around its position) and 35 Å, while those of CH_4 and CO_2 fluctuate, respectively, between 1 Å and 10 Å, and 1 Å and 8 Å. These features are all consistent with the hopping mechanism that is often invoked to explain diffusion of small gas molecules in amorphous materials. According to the hopping mechanism, the gas molecules oscillate in a cavity until the *tunnels* between adjacent cavities are opened, which allow them to hop to the neighboring cavities, provided that they are not already occupied by other gas molecules. The magnitude of the oscillations and the frequency of the hops from one cavity to another depend on the material's density and morphology.

Figure 14 presents the logarithmic plots of the mean-square displacements of the three gases versus time at 273 K, computed in the (*NPT*) ensemble. In the Fickian regime of diffusion, a plot of $\log\langle R^2(t)\rangle$ versus time $\log t$ should eventually become a straight line with a slope of 1. In all the cases, the slopes are indeed $\simeq 1$. The estimated diffusivities of

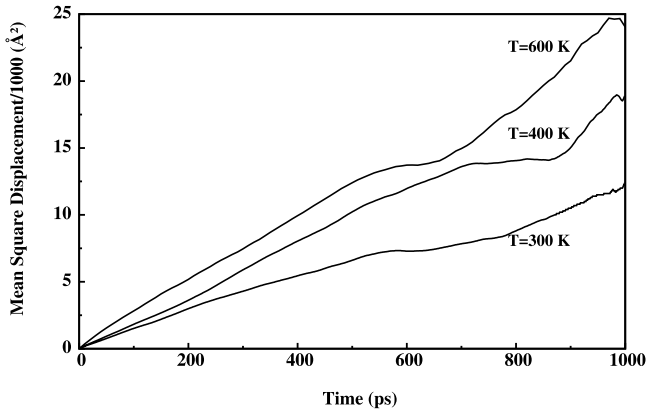

FIG. 15. Time- and temperature-dependence of the mean-square displacements of H_2, computed in the (*NPT*) ensemble.

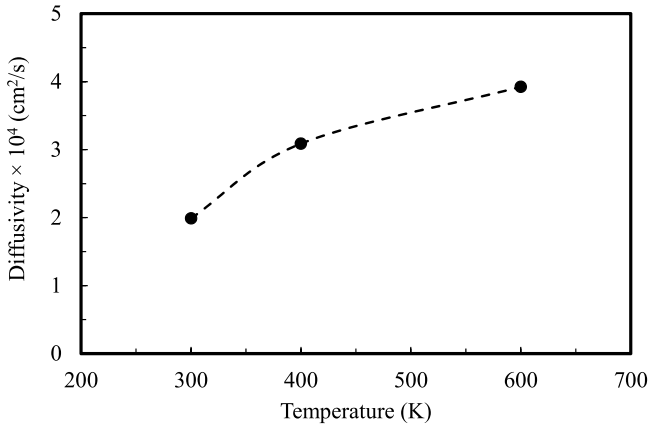

FIG. 16. Temperature-dependence of self-diffusivity of H_2 in the model amorphous SiC film.

the three gases are listed in Table II. The estimates are all in the range of diffusivities of small gas molecules in amorphous materials.

Since separation of hydrogen from a gaseous mixture by SiC membranes is of prime interest to us, we computed its effective diffusivities at three temperatures that are encountered in practical applications of amorphous SiC as a membrane. The results for the mean-square displacements are shown in Fig. 15, while Fig. 16 presents temperature-dependence of the diffusivity of H_2 in the amorphous SiC film.

VII. SUMMARY

Based on the reactive force field ReaxFF, we described a first principles-based multiparadigm, multiscale strategy for simulating complex materials fabrication processes involving chemical reactions, which yields both the final material structure and other products of the processes. As an example, we simulated thermal decomposition of the polymer HPCS in order to generate an atomistic model of amorphous SiC film, a practice that is followed in the preparation of SiC nanoporous membranes. All the reaction products of the thermal decomposition of the polymer agree with the experimental data.[33] Using extensive molecular dynamics simulations, we also calculated the structural and transport properties of the amorphous SiC film. Elsewhere,[40] where we reported the results of our preliminary MD simulations, we showed that the computed radial distribution function and x-ray diffraction pattern of the amorphous SiC film agree with the experimental data. Thus, the proposed methodology is a powerful tool for atomistic modeling of formation of complex materials that involve chemical reactions. The application of the method to SiC nanoporous membranes[33] was recently reported elsewhere.[52]

ACKNOWLEDGMENTS

Work at USC was supported by the DOE and NSF. We thank Lianchi Liu for helpful discussions.

[1]A. W. Weimer, *Carbide, Nitride, and Boride Materials: Synthesis and Processing* (Springer, Berlin, 1997).
[2]M. S. Shur, S. L. Rumyantsev, and M. Levinshtein, *SiC Materials and Devices* (World Scientific, Singapore, 2006).
[3]V. Suwanmethanond, E. Goo, P. K. T. Liu, G. Johnston, M. Sahimi, and T. T. Tsotsis, Ind. Eng. Chem. Res. **39**, 3264 (2000); R. Ciora, B. Fayyaz, P. K. T. Liu, V. Suwanmethanond, R. Mallada, M. Sahimi, and T. T. Tsotsis, Chem. Eng. Sci. **59**, 4957 (2004); B. Elyassi, M. Sahimi, and T. T. Tsotsis, J. Membr. Sci. **288**, 290 (2007); **316**, 73 (2008); B. Elyassi, W. Deng, M. Sahimi, and T. T. Tsotsis, Ind. Eng. Chem. Res. **52**, 10269 (2013).
[4]O. M. Yaghi, M. O'Keeffe, N. W. Ockwig, H. K. Chae, M. Eddaoudi, and J. Kim, Nature **423**, 705 (2003); A. P. Cote, A. I. Benin, N. W. Ockwig, M. O'Keeffe, A. J. Matzger, and O. M. Yaghi, Science **310**, 1166 (2005).
[5]B. Elyassi, T. W. Kim, M. Sahimi, and T. T. Tsotsis, Mater. Chem. Phys. **118**, 259 (2009); K. Malek and M. Sahimi, J. Chem. Phys. **132**, 014310 (2010); S. H. Barghi, T. T. Tsotsis, and M. Sahimi, Int. J. Hydrogen Energy **39**, 21107 (2014).
[6]Q. Liu, H.-J. Wu, R. Lewis, G. E. Maciel, and L. V. Interrante, Chem. Mater. **11**, 2038 (1999); L. V. Interrante, K. Moraes, L. MacDonald, and W. Sherwood, "Mechanical, thermochemical, and microstructural characterization of AHPCS-derived SiC," in *Advanced SiC/SiC Ceramic Composites: Developments and Applications in Energy Systems*, edited by A. Kohyama, M. Singh, H.-T. Lin, and Y. Katoh (John Wiley & Sons, Inc., Hoboken, NJ, USA, 2006), Vol. 144, p. 123.
[7]K. Farah, F. Müller-Plathe, and M. C. Böhn, ChemPhysChem **13**, 1127 (2012).
[8]A. C. T. van Duin, S. Dasgupta, F. Lorant, and W. A. Goddard, J. Phys. Chem. A **105**, 9396 (2001); A. C. T. van Duin, A. Strachan, S. Stewman, Q. Zhang, X. Xu, and W. A. Goddard, *ibid.* **107**, 3803 (2003); A. C. T. van Duin, Y. Zeiri, F. Dubnikova, R. Kosloff, and W. A. Goddard, J. Am. Chem. Soc. **127**, 11053 (2005); S. Cheung, W. Q. Deng, A. C. T. van Duin, and W. A. Goddard, J. Phys. Chem. A **109**, 851 (2005); K. D. Nielson, A. C. T. van Duin, J. Oxgaard, W. Q. Deng, and W. A. Goddard, *ibid.* **109**, 493 (2005); L. Liu, A. Jaramillo-Botero, W. A. Goddard, and H. Sun, *ibid.* **116**, 3918 (2012); K. Chenoweth, A. C. T. van Duin, P. Persson, M. J. Cheng, J. Oxgaard, and W. A. Goddard, J. Phys. Chem. C **112**, 14645 (2008); A. Strachan, A. C. T. van Duin, D. Chakraborty, S. Dasgupta, and W. A. Goddard, Phys. Rev. Lett. **91**, 098301 (2003).
[9]D. W. Brenner, Phys. Rev. B **42**, 9458 (1990); D. W. Brenner, O. A. Shenderova, J. A. Harrison, S. J. Stuart, B. Ni, and S. B. Sinnott, J. Phys.: Condens. Matter **14**, 783 (2002).
[10]M. R. Nyden and D. W. Noid, J. Phys. Chem. **95**, 940 (1991).
[11]J. Tersoff, Phys. Rev. Lett. **56**, 632 (1986); Phys. Rev. B **38**, 9902 (1988); **37**, 6991 (1988); **39**, 5566 (1989).
[12]F. H. Stillinger and T. A. Webber, J. Phys. Chem. **91**, 4899 (1987); J. Chem. Phys. **88**, 5123 (1988); Phys. Rev. Lett. **62**, 2144 (1989); H. Feil, J. Dieleman, and B. J. Garrison, J. Appl. Phys. **74**, 1303 (1993); D. E. Hanson, J. D. Kress, and A. F. Voter, J. Chem. Phys. **110**, 5983 (1999).
[13]K. Chenoweth, S. Cheung, A. C. T. van Duin, W. A. Goddard, and E. M. Kober, J. Am. Chem. Soc. **127**, 7192 (2005).
[14]T. G. Desai, J. W. Lawson, and P. Keblinski, Polymer **52**, 577 (2011).
[15]B. Saha and G. C. Schatz, J. Phys. Chem. B **116**, 4684 (2012).
[16]Jaguar 5.5, Schrödinger, LLC, Portland, Oregan, 1991-2003.
[17]A. D. Becke, J. Chem. Phys. **98**, 1372 (1993).
[18]R. Krishnan, J. S. Binkley, R. Seeger, and J. A. Pople, J. Chem. Phys. **72**, 650 (1980); T. Clark, J. Chandrasekhar, G. W. Spitznagel, and P. V. R. Schleyer, J. Comput. Chem. **4**, 294 (1983).
[19]P. C. Haharan and J. A. Pople, Theor. Chim. Acta **28**, 213 (1973); M. M. Francle, W. J. Pietro, W. J. Hehre, J. S. Binkley, M. S. Gordon, D. J. DeFrees, and J. A. Pople, J. Chem. Phys. **77**, 3654 (1982).
[20]P. Giannozzi *et al.*, J. Phys.: Condens. Matter **21**, 395502 (2009).
[21]J. P. Perdew, K. Burke, and M. Ernzerhof, Phys. Rev. Lett. **77**, 3865 (1996).
[22]J. P. Perdew, A. Chevary, S. A. Vosko, K. A. Jackson, M. R. Pederson, D. J. Singh, and C. Fiolhais, Phys. Rev. B **46**, 6671 (1992).
[23]H. J. Monkhorst and J. D. Pack, Phys. Rev. B **13**, 5188 (1976).
[24]A. Jaramillo-Botero, S. Naserifar, and W. A. Goddard III, J. Chem. Theory Comput. **10**, 1426 (2014).
[25]J. J. P. Stewart, J. Comput. Chem. **10**, 209 (1989).
[26]D. N. Theodorou and U. W. Suter, Macromolecules **18**, 1467 (1985); E. Tocci, D. Hofmann, D. Paul, N. Russo, and E. Drioli, Polymer **42**, 521 (2001).
[27]M. M. Ostwal, T. T. Tsotsis, and M. Sahimi, Phys. Rev. E **79**, 061801 (2009).
[28]A. R. Mehrabi and M. Sahimi, Phys. Rev. Lett. **82**, 735 (1999).
[29]N. Kim, A. Harale, T. T. Tsotsis, and M. Sahimi, J. Chem. Phys. **127**, 224701 (2008); A. R. Mehrabi and M. Sahimi, *ibid.* **128**, 234503 (2008).
[30]D. Wolf, P. Keblinski, S. R. Phillpot, and J. Eggebrecht, J. Chem. Phys. **110**, 8254 (1999).

[31]H. C. Andersen, J. Chem. Phys. **72**, 2384 (1980).
[32]S. Nosé, J. Chem. Phys. **81**, 511 (1984); W. Hoover, Phys. Rev. A **31**, 1695 (1985).
[33]L. V. Interrante, C. W. Whitmarsh, and W. Sherwood, MRS Proc. **346**, 595 (1994).
[34]H. Q. Ly, R. Taylor, R. J. Day, and F. Heatley, J. Mater. Sci. **36**, 4045 (2001).
[35]X. Tang, L. Zhang, H. Tu, H. Gu, and L. Chen, J. Mater. Sci. **45**, 5749 (2010).
[36]P. Patnaik, *Handbook of Inorganic Chemicals* (McGraw-Hill, New York, 2002).
[37]S. Naserifar, L. Liu, W. A. Goddard, T. T. Tsotsis, and M. Sahimi, J. Phys. Chem. C **117**, 3308 (2013).
[38]See http://www.starfiressystems.comfor Starfire Systems, Inc.; accessed 10 January 2013.
[39]Cerius2, version 4.0, Accelyrs, San Diego, 1999.
[40]Y. Goldberg, M. E. Levinshtein, and S. L. Rumyantsev, *Properties of Advanced Semiconductor Materials: GaN, AIN, InN, BN, SiC, SiGe*, edited by M. E. Levinshtein, S. L. Rumyantsev, and M. S. Shur (Wiley, New York, 2001), p. 93.
[41]S. Naserifar, W. A. Goddard, L. Liu, T. T. Tsotsis, and M. Sahimi, J. Phys. Chem. C **117**, 3320 (2013).
[42]X.-Y. Tang, L. Zhang, H. B. Tu, H. Gu, and L. F. Chen, J. Mater. Sci. **45**, 5749 (2010).
[43]M. Ishimaru, I.-T. Bae, Y. Hirotsu, S. Matsumura, and K. E. Sickafus, Phys. Rev. Lett. **89**, 055502 (2002).
[44]M. G. Sedigh, W. J. Onstot, L. Xu, W. L. Peng, T. T. Tsotsis, and M. Sahimi, J. Phys. Chem. A **102**, 8580 (1998); M. G. Sedigh, L. Xu, T. T. Tsotsis, and M. Sahimi, Ind. Eng. Chem. Res. **38**, 3367 (1999); M. G. Sedigh, M. Jahangiri, P. K. T. Liu, M. Sahimi, and T. T. Tsotsis, AIChE J. **46**, 2245 (2000).
[45]A. K. Rappe, A. J. Casewit, K. S. Colwell, W. A. Goddard, and W. M. Skiff, J. Am. Chem. Soc. **114**, 10024 (1992).
[46]H.-Q. Ding, N. Karasawa, and W. A. Goddard, J. Chem. Phys. **97**, 4309 (1992).
[47]M. Tanemura, T. Ogawa, and N. Ogita, J. Comput. Phys. **51**, 191 (1983).
[48]S. Y. Lim, T. T. Tsotsis, and M. Sahimi, J. Chem. Phys. **119**, 496 (2003); S. Y. Lim, M. Sahimi, T. T. Tsotsis, and N. Kim, Phys. Rev. E **76**, 011810 (2007).
[49]A. K. Doolittle, J. Appl. Phys. **22**, 1471 (1951).
[50]J. Budzien, J. D. McCoy, and D. B. Adolf, J. Chem. Phys. **119**, 9269 (2003).
[51]M. H. Cohen and D. Turnbull, J. Chem. Phys. **31**, 1164 (1959); D. Turnbull and M. H. Cohen, *ibid.* **34**, 120 (1961).
[52]S. Naserifar, W. A. Goddard, T. T. Tsotsis, and M. Sahimi, J. Membr. Sci. **473**, 85 (2015).